Interaction between nanoparticles and charged phospholipid membrane

Journal:	*Physical Chemistry Chemical Physics*
Manuscript ID	CP-ART-07-2018-004740.R1
Article Type:	Paper
Date Submitted by the Author:	10-Oct-2018
Complete List of Authors:	Bohinc, Klemen; Faculty of Health Sciences, University of Ljubljana Huang, Beibei; The University of Texas MD Anderson Cancer Center Tan, Zhi; MD Anderson Cancer Center Zhang, Shuxing; UT MD Anderson Cancer Center , Department of Experimental Therapeutics

Journal Name

ARTICLE TYPE

Cite this: DOI: 10.1039/xxxxxxxxxx

Interaction between Nanoparticles and Charged Phospholipid Membrane

Beibei Huang [a], Zhi Tan [a], Klemen Bohinc [b*†] and Shuxing Zhang[a*‡]

Received Date
Accepted Date

DOI: 10.1039/xxxxxxxxxx

www.rsc.org/journalname

Charged lipids in cell membranes and subcellular organelles are arranged in the form of a bilayer with the hydrocarbon tails sequestered away from the water and the polar head groups exposed to the aqueous environment. Most of their bear net negative charges leading to the negatively charged cell membranes. Charged lipid-lipid and lipid-protein interactions are generally dynamic and heavily depend on their local molecular concentrations. To examine the electrostatic properties of charged lipid layers in contact with an electrolyte solution, we incorporate the Single Chain Mean Field theory with Poisson Boltzmann theory to explore the equilibrium structure of charged phospholipid membranes. Using the three beads coarse-grained model we reproduced the essential equilibrium properties of the charged phospholipid bilayer. We also investigate the influence of the mobile ions on the thickness of the layer, the area per lipid (APL), and the electrostatic potential of the membrane. Then we investigate the attraction-repulsion property of two charged nanoparticles which are stuck on the charged lipid molecules surrounded with mobile ions. After that we simulated the interaction between Pleckstrin homology domain (PH domain) of Akt and cytoplasmic membrane. Taking into account the electrostatic interaction, we observe the structure changes of the membrane under different concentration of mobile ions in its equilibrium state. Also we discuss the influence of mobile ions on the size of the pore opened in the membrane by the charged protein. Such observation may shed a light on the activation of oncogenic Akt (or protein kinase B) around the membrane at the molecular level.

1 Introduction

Natural lipid bilayers make up the cell membranes of almost all living organisms, and they separate the contents of cells from their extracellular surroundings. For example, plasma membrane lipids are 7.9% red-blood-cell (RBC) phosphatidylserine (PS) by weight in humans and 10.6% RBC PS by weight in pigs[1]. Phospholipid membranes are complex and heterogeneous objects consisting of phospholipid molecules, each molecule with one hydrophilic head and two hydrophobic tails. Charged lipids in the cell membranes and subcellular organelles are arranged in the form of a bilayer with the hydrocarbon tails sequestered away from the water and the polar head groups exposed to the aqueous environment. One basic function of lipids in a biomembrane is to compartmentalize the space. Most charged lipids bear a net negative charge, and most charged cell membranes are therefore usually negatively charged surfaces. Molecular bioavailability and toxicity have long been linked to the ability of chemicals to permeate cell membranes. Membrane permeability has thus attracted increasing attention from the biological and environmental sciences[2–5]. Research on charged lipid membranes is scarce despite they are of such importance. Dysfunctions of lipid membranes have also been implicated in many diseases including cancer[6–8]. More recently, the translocation of nanoparticles with tunable degrees of hydrophobicity through lipid bilayer membranes was studied and showed that molecular machines can drill holes in cell membranes[9,10]. These findings may also have applications in the field of drug development[11–14].

Many of the membrane's structural properties and functions depend on electrostatic interactions[15] such as structural stability and lateral phase transitions. Functionally, lipid bilayers act as barriers that control the flow and localization of ions, proteins, and other molecules. Lipid bilayers allow certain molecules or ions to pass through them by either passive transport (including diffusion and facilitated diffusion) or active transport[16,17].

Lipid headgroups are charged or zwitterionic. Electrostatic charge is a key property of lipid molecules, determining their physicochemical properties, structures, and biological functions. Lipid membranes in aqueous solutions form an electrostatic double layer, the result of ion distribution close to the membrane. The standard description of the double layer is based on the continuum mean-field approximation and is commonly referred to as the Poisson-Boltzmann (PB) theory[18–21]. Central to the PB theory is the PB equation with appropriate boundary conditions, of which the solution determines the electrostatic potential. PB formalism has frequently been used to describe membrane electrostatics both qualitatively and quantitatively[22]. Lipowsky[23] et al. analyzed electrostatic properties of membranes based on the PB theory. Their study presented specific solutions of the problems with a single flat and rigid membrane, generalized to two flat membranes, and then considered flexible membranes in various situations including single membranes, double membranes, and stacks of several membranes. The coupling between the electrostatic and elastic properties was emphasized in the discussion of these flexible, charged membranes. Bohinc[20] et al. derived an analytic expression for the dipole potential of a single lipid layer using an electrostatic model that is based on an extended version of the linearized PB theory. Levin[24] reviewed the thermodynamic consequences of electrostatic correlations in a variety of systems ranging from classical plasmas to molecular biology and introduced an application of electrostatic correlations in gene therapy. Due to the enormous configurational space and high number of interactions, computer simulation of lipid bilayers has been challenging for decades,[25,26] with full-atomistic molecular dynamics methods limited to microseconds and lengths of nanometers[25].

The membrane-mediated interaction between proteins has been studied. A simple example of such studies is the interaction between two cylindrical inclusions in a symmetric lipid bilayer. The theory takes into account two contributions to the free energy, the elastic behavior of the membrane and the conformational restrictions that the flexible hydrocarbon chains of the lipids experience in the vicinity of a rigid inclusion[27]. It was found that the short-range interaction potential between two cylindrical inclusions depends on the degree of hydrophobic mismatch and on the spontaneous curvature of the lipid layers. Andrey[28] proposed a theoretical models for DNA condensation on cationic lipid membranes, examined the conditions of full wrapping of a cylindrical DNA-like semi-flexible polyelectrolyte by an oppositely charged membrane, self-consistently analyzed the shape and the extent of the membrane for two parallel DNA rods. Andrey[29] also investigated extensive computer simulations mutual interactions of rod-like particles adsorbed on the surface of responsive elastic two-dimensional sheets, that unveiled the phase diagram of attractive-repulsive rod-rod interactions in the plane of their separation and mutual orientation.

More recently Seo[30] proved positively charged divalent and multivalent cations accumulate around the negatively charged PIP2 (phosphatidylinositol 4,5-bisphosphate) inhibit electrostatic PIP2-PLC (phospholipase C) interaction due to electrostatic charge shielding effect. In the context of the cell membrane, the apparent membrane electrostatic charge is substantially reduced as a result of the ion shielding effect[31]. These findings enlighten us to quantitatively explore the role of mobile ions in the electrostatic interactions between charged membrane and protein or charged nanoparticles.

In computer simulation schemes, such as Monte Carlo (MC) and molecular dynamics (MD) simulations, coarse-grained models of phospholipids have been proposed to reduce the degrees of freedom of the system[32–38]. However, even in coarse-grain models, MC and

[a] *Intelligent Molecular Discovery Laboratory, Department of Experimental Therapeutics, The University of Texas M. D. Anderson Cancer Center, 1901 East Road, Houston, TX 77054, USA*

[b] *Faculty of Health Sciences, University of Ljubljana, 1000 Ljubljana, Slovenia*

† Correspondence. EM: klemen.bohinc@zf.uni-lj.si, Phone: +38613001170

‡ Correspondence. EM: shuzhang@mdanderson.org, Phone: +17137452958

MD simulations are inefficient if only equilibrium properties are considered when the free energy of the whole system is at a minimum. To avoid expensive equilibration processes in MC and MD simulations,[39] adopted Single Chain Mean Field (SCMF) was proposed to simulate the equilibrium structure of phospholipid membranes at the molecular level. SCMF combines the self-consistent mean-field theory with the conformational variability accessible in MC simulations[40–42]. This method can be seen as solving a constrained Monte Carlo nonlinear optimization problem, with the solution of the nonlinear SCMF equations corresponding to the minimum free energy. The accuracy of the method is comparable with that of MC simulations, while the speed is dominated by the speed of the nonlinear solver. It is worth pointing out that the Mean-field theory which was applied in Boltzmann machine learning at the end of last century has become popular in the field of deep learning, and comparison of functional forms for energy of Restricted Boltzmann Machine and SCMF reveal closer homologous relationship in method[43,44].

In this paper we applied SCMF theory incorporated with PB theory to simulate charged phospholipid membranes. Using the simulation results, we explored the influence on the equilibrium properties of charged phospholipid membranes in two aspects(a schematic presentation is shown in Fig.1 We adopt 3-beads model since it is the simpler due to less restricted conformational space, and it demands less computer resources to simulate the charged phospholipid membranes.). First aspect is the quantity of electric charge carried on lipids which is represented by the surface charge density, and the second is the salt concentration in the solution. Based on our new theory we propose a framework to simulate the interaction between the charged membrane and nanoparticle or protein (the framework is described in Fig.2). Finally, as an application, we simulate the interaction between the Akt Pleckstrin Homology (PH) domain and the cytoplasmic membrane, taking into account electrostatic interactions. As part of this application we formally discuss the equilibrium state of the structure of the complex and the influence of mobile ions on the size of the opened membrane pore.

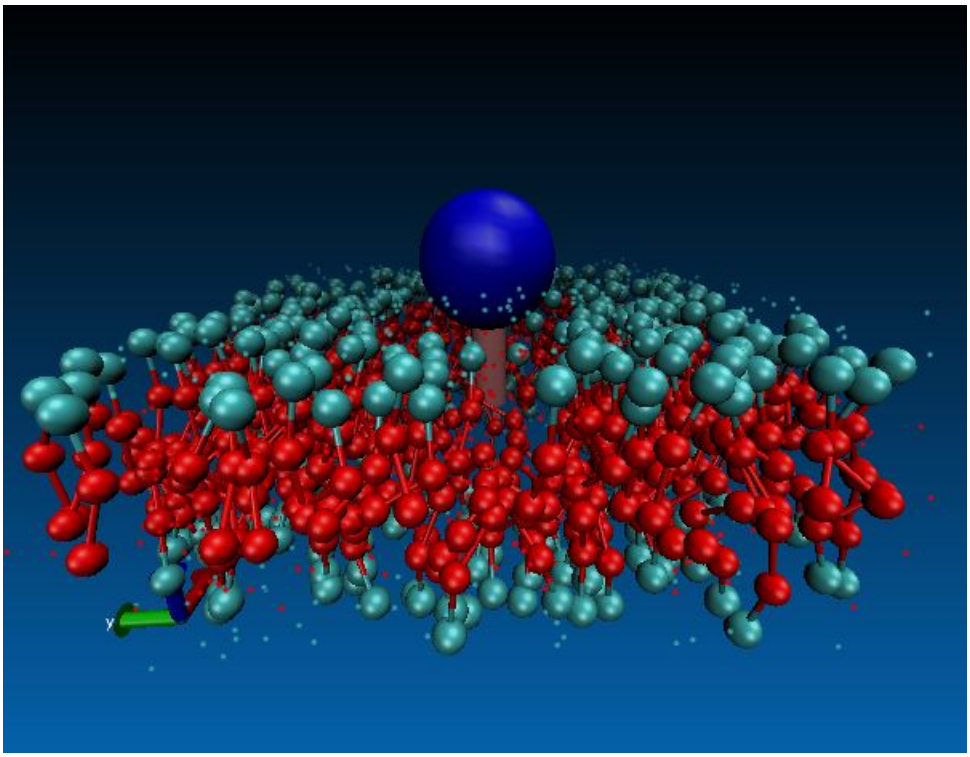

Fig. 1 Schematic presentation of the interaction between the charged membrane and a charged nanoparticle or protein. In this three-bead model (HTT), the membrane lipids are represented by a teal bead (charged group) and two red beads (uncharged/nonionic groups). The charged nanoparticle or protein is represented by a purple sphere, while the attached pink cylinder represents phosphatidylinositol phosphate inserted into the membrane. The small cyan and red points permeating the membrane and surrounding the protein are mobile ions.

2 Single Chain Mean Field With Poisson Boltzmann Theory

2.1 Physical Model of The Charged Phospholipid

The SCMF theory was originally developed for the micellization problem of low molecular surfactants. This theory describes a single molecule in the molecular fields[40,41,45] and has been used to describe the phospholipid membranes[39]. We start from the coarse grained models of lipid Dimyristoylphosphatidylcholine (DMPC) proposed in Pogodin[39] et al., in which hydrophobic units and hydrophilic units, and the solvent molecules are represented by beads of the same size and interaction range.

In our three beads coarse-grained model, P denotes the phospholipid molecule, S denotes the solvent molecule, and i_ω denotes the mobile monovalent ions with the valency $\omega = \pm$. In the particular phospholipid molecule T and H denote hydrophobic and hydrophilic

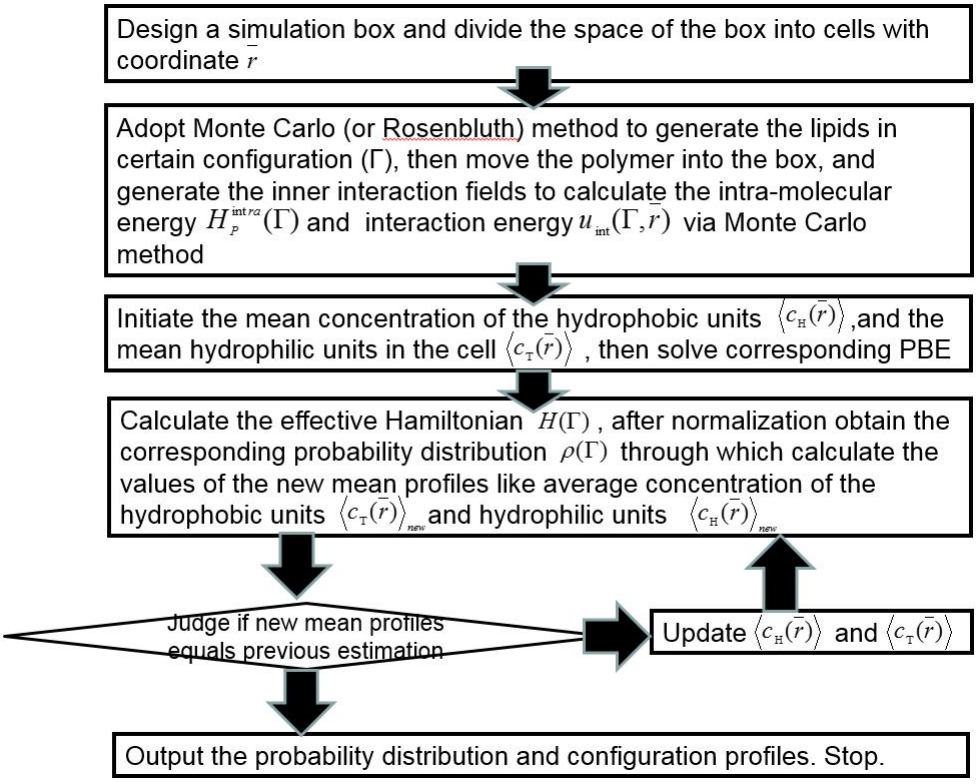

Fig. 2 The framework to simulate the interaction between charged membrane and protein or nanoparticle

beads respectively. Therefore the phospholipid molecule is described by freely joining two hydrophobic beads and one hydrophilic bead which is schematically represented as HTT.

One of a typical charged lipids in the membrane is phosphatidylserine (DPPS) which not only provides an environment for proteins to work in but is also involved in modulating the structure and function of those proteins[46]. Since DPPS and DMPC are of high similarity in structure except that the headgroup of DPPS is charged, we model the DPPS lipids in the same way as DMPC. Furthermore it can be adapted to other similar lipid model by adjusting the corresponding properties.

We assume that the heads of the type H in the phospholipid molecules carry charge, hence the phospholipid molecules are treated as linear polyelectrolytes on which the charge is evenly distributed. Once phospholipid molecules self-assemble we obtain the charged surface of the phospholipid membrane in contact with the solution. In our model, the mobile salt ions in the solution are point-like.

2.2 Application to the Charged Phospholipid Membranes

In the theory, the free energy F of a system with the volume V containing N_P charged phospholipid chains consists of four terms:

$$F = \langle H_{\text{intra}}\rangle + \langle H_{\text{inter}}\rangle + \langle H_{\text{el}}\rangle - \langle S\rangle \ . \tag{1}$$

The first term H_{intra} in Eq.1 is the energy generated from the short range interactions between beads inside the same molecule. In the second term H_{inter} the energy is generated from the hydrophobic and hydrophilic interactions between the beads of different phospholipid molecules and solvent. The contribution originated from the long range electrostatic interaction between charged phospholipid molecules is included in the third term H_{el}. The last term S corresponds to the entropy of the system composed of phospholipid molecules, solvent and mobile ions. The angular brackets denote the average value over the probability distribution function (pdf) of a single phospholipid molecule $\rho(\Gamma)$, where Γ denotes the conformation state of the phospholipid molecule in the membrane. With the notations introduced in previous section 2.1, we denote the bead type H and T by α, and the average concentration of the beads of the $\alpha-$th types can be defined by

$$\langle c_\alpha(\mathbf{r})\rangle = \int c_\alpha(\Gamma,\mathbf{r})\rho(\Gamma)d\Gamma \tag{2}$$

where $c_\alpha(\Gamma,\mathbf{r})$ is the concentration of the beads of the $\alpha-$th type of a phospholipid molecule in the conformation state Γ at the position $\mathbf{r}$. In Eq.2 we integrate over all possible conformation states at the position $\mathbf{r}$.

2.2.1 Entropy contribution

Our system includes three components: charged phospholipid molecules of concentration c_P, solvent molecules of concentration $c_s(\mathbf{r})$ and monovalent mobile ions of concentration $c_{i\omega}(\mathbf{r})$, $\omega = \pm$ at r . The entropy term can be written as

$$\langle S \rangle = N_P \left\langle \ln \frac{\rho N_P}{e} \Lambda_P \right\rangle + \int d\mathbf{r} \left\{ c_S(\mathbf{r}) \ln \frac{c_S(\mathbf{r})}{e} \Lambda_S \right\} + \sum_{\omega=\pm} \int d\mathbf{r} \left\{ c_{i\omega}(\mathbf{r}) \ln \frac{c_{i\omega}(\mathbf{r})}{e} \Lambda_{i\omega} \right\} \tag{3}$$

where the angular brackets in the first term denotes the average over single phospholipid molecule pdf, and Λ_α denotes the de Broglie lengths of corresponding beads, $\alpha \in P,S$ and $i\pm$.

2.2.2 Intra-molecular energy

The intra-molecular energy of the system can be written as a sum over the single phospholipid molecule:

$$\langle H_{intra} \rangle = N_P \left\langle H_P^{intra} \right\rangle \tag{4}$$

where N_P is the number of phospholipid molecules which are assembled into the membrane. In our model the intra-molecular energy originates from the intramolecular nonbonded hydrophobic beads (T-T) interactions[45,47,48].

2.2.3 Inter-molecular Energy

The short range Inter-molecular energy between a phospholipid molecule in the conformation state Γ and another phospholipid molecule in the conformation state Γ', is actually the interaction between the beads of $\alpha-$th type of phospholipid molecule in the conformation state Γ and the beads of $\beta-$th type of phospholipid molecule in the conformation state Γ', and it can be written as

$$H^{inter}(\Gamma,\Gamma') = \sum_{\alpha,\beta} \int u_{int}^{\alpha}(\Gamma,\mathbf{r}) c_\beta(\Gamma',\mathbf{r}) d\mathbf{r} \tag{5}$$

where $u_{int}^{\alpha}(\Gamma,\mathbf{r})$ denotes the field potential created by the beads of $\alpha-$th type in the phospholipid molecules in the conformation state Γ at $\mathbf{r}$, and $c_\beta(\Gamma',\mathbf{r})$ is the concentration of the beads of $\beta-$th type in the phospholipid molecules in the conformation state Γ' at $\mathbf{r}$.

We still consider the membrane that is assembled by N_P phospholipids. The average inter-molecular free energy that accounts for the interaction between different phospholipids and interactions between phospholipid and solvent can be written in the form

$$\langle H_{inter} \rangle = \sum_{\alpha,\beta} \frac{N_P(N_P-1)}{2} \int d\mathbf{r} \left\{ \langle u_{int}^{\alpha}(\mathbf{r}) \rangle \langle c_\beta(\mathbf{r}) \rangle \right\} + \sum_{\alpha} N_P \int d\mathbf{r} \left\{ \langle u_{int}^{\alpha}(\mathbf{r}) \rangle c_s(\mathbf{r}) \right\} \tag{6}$$

where $\langle u_{int}^{\alpha}(\mathbf{r}) \rangle$ is the average fields created by the beads of $\alpha-$th type, and $\langle c_\beta(\mathbf{r}) \rangle$ denotes the average concentration of beads of $\beta-$th type. The first term minus one is due to the exclusion of the intra-molecular energy of which both the concentration and field come from the same molecule. The first term accounts for the interaction between beads of $\alpha-$th type and beads of $\beta-$th type of different phospholipid molecules, and similarly the second term accounts for the interaction between corresponding beads and the solvent. It is noted $\alpha-$th type and $\beta-$th type that can be either type H or type T, and practically in our model for phospholipid membrane assembly we only consider interactions between four type pairs of bead's type: (1) H and H, (2) T and T, (3) H and S, (4) T and S. Besides we adopt the approximation $\int d\mathbf{r} \left[u_{int}^{H}(\Gamma,\mathbf{r}) \langle c_H(\mathbf{r}) \rangle + u_{int}^{T}(\Gamma,\mathbf{r}) \langle c_T(\mathbf{r}) \rangle \right] \approx \int d\mathbf{r} \left[\langle u_{int}^{H}(\mathbf{r}) \rangle c_H(\Gamma,\mathbf{r}) + \langle u_{int}^{T}(\mathbf{r}) \rangle c_T(\Gamma,\mathbf{r}) \right]$, since we assume the beads of all types are of the same size.

2.2.4 Electrostatic contribution and Poisson-Boltzmann equation

The third term $\langle H_{el} \rangle$ on the right-hand side of Eq.1 is the contribution of electrostatic interaction, which results from the Coulomb forces interaction between charged phospholipids, as well as the screening effect from mobile ions in solution that has been already considered in the entropy contribution Eq.(3)

$$\langle H_{el} \rangle = \frac{1}{2} \int d\mathbf{r} \left\{ \langle \rho_{total}(\mathbf{r}) \rangle \varphi(\mathbf{r}) \right\} \tag{7}$$

where $\varphi(\mathbf{r})$ is the electrostatic potential at $\mathbf{r}$. In a mean-field approach, the essential input to calculate the electrostatic contribution that accounts for the effective interaction, is the electrostatic mean-field potential which can be obtained from a Poisson-Boltzmann equation[49–51], in which the steric effect of charged phospholipid molecules or excluded volume interaction between them are neglected[52,53], hence it can be treated as a supplementary contribution for the total free energy of the charged system. We define the total charge

density as $\langle \rho_{total}(\mathbf{r}) \rangle$

$$\langle \rho_{total}(\mathbf{r}) \rangle = \int d\Gamma \left\{ \left[c_H(\Gamma,\mathbf{r})\lambda_H + c_T(\Gamma,\mathbf{r})\lambda_T \right] \rho(\Gamma) \right\} + c_\infty \left(e^{-\beta q \varphi(\mathbf{r})} - e^{\beta q \varphi(\mathbf{r})} \right) \tag{8}$$

where the first term denotes the fixed density of the charge on hydrophobic and hydrophilic beads, and λ_H and λ_T denotes the weight density on particular beads. The second term is the contribution of the monovalent mobile ions, c_∞ denotes the bulk concentration of mobile ions in the solution. $\beta = e/kT$ where e is the elementary charge, kT is the product of the Boltzmann constant, k, and the temperature T. In addition $c_{\kappa l_B} = (\kappa l_B)^2 = 8\pi c_\infty l_B^3$ is in proportion to the salt density, where l_B is Bjerrum length (Supporting Information SI-15.1). Hence we use c_∞ as a control parameter tuning the salt density in the solution in following discussion.

Let us note that Eq.(8) connects the microscopic properties of the individual phospholipid ($c_H(\Gamma,\mathbf{r})\lambda_H + c_T(\Gamma,\mathbf{r})\lambda_T$) to the macroscopic charge density $\langle \rho_{total}(\mathbf{r}) \rangle$ through the sum of the concentrations of phospholipid in certain configuration Γ. We insert $\langle \rho_{total}(\mathbf{r}) \rangle$ into the Poisson equation and obtain the differential Poisson-Boltzmann equation

$$\nabla^2 \varphi(\mathbf{r}) = -\frac{4\pi q}{\varepsilon} \langle \rho_{total}(\mathbf{r}) \rangle \tag{9}$$

where ε is the uniform dielectric constant. The solution procedure for the Poisson Boltzmann equation is given in Supporting Information SI-15.1 and SI-25.2. The Poisson-Boltzmann equation is a differentiate equation for the electrostatic potential $\varphi(\mathbf{r})$. The concentrations of monovalent mobile ions $c_{i\omega}(\mathbf{r})$ are obtained from Boltzmann relation $\ln[c_{i\omega}(\mathbf{r})/c_\infty] = -\omega\varphi(\mathbf{r})$, where $\omega = \pm$.

2.2.5 Self-consistent Calculation of Free Energy

Finally we can obtain the total free energy by substituting the four contributions Eqs. (3,4,6 and 7) into the Eq.(1). In addition we consider the incompressibility condition at $\mathbf{r}$

$$\langle \phi_H(\mathbf{r}) \rangle + \langle \phi_T(\mathbf{r}) \rangle + \phi_S(\mathbf{r}) = \phi_0 \tag{10}$$

where $\langle \phi_H(\mathbf{r}) \rangle$ and $\langle \phi_T(\mathbf{r}) \rangle$ denote the corresponding mean volume fraction of beads H and T respectively. $\phi_S(\mathbf{r}) = c_S(\mathbf{r})v_s$ is the volume fraction of the solvent at $\mathbf{r}$, $c_S(\mathbf{r})$ denotes the corresponding concentration. ϕ_0 is the total volume fraction occupied by the molecules in the box, and it is noted that its value is less than 1.0 due to the space between molecules.

v_s denotes the volume of one solvent bead and we assume the linear relation between the concentration of bead of type α and corresponding volume fraction $\phi_\alpha(\mathbf{r}) = c_\alpha(\mathbf{r})v_s$. Hence via Eqs.(2) self-consistency condition for volume fraction of bead of type α Eqs.(11) still hold

$$\langle \phi_\alpha(\mathbf{r}) \rangle = \int \rho(\Gamma)\phi_\alpha(\Gamma,\mathbf{r}) d\Gamma \tag{11}$$

where α is the bead in the molecules of the conformation state Γ, and it can be of type H or T.

Lagrange multiplier $\pi(\mathbf{r})$ is introduced for constraint condition Eq.(10) to the total free energy in Eq.(1) to obtain the augmented free energy $F_{aug} = F + \pi(\mathbf{r}) \int d\mathbf{r} \left\{ \langle \phi_H(\mathbf{r}) \rangle + \langle \phi_T(\mathbf{r}) \rangle + \phi_S(\mathbf{r}) - \phi_0 \right\}$, and then we minimize it respect to the concentration of the solvent $c_s(\mathbf{r})$ to get the approximate expression for the Lagrange multiplier $\pi(\mathbf{r})$

$$\pi(\mathbf{r}) \quad \approx \quad -\frac{\ln \phi_s(\mathbf{r})}{v_s} \tag{12}$$

Substitution of Eq.(12) into F_{aug} and minimization of F_{aug} with respect to $\rho(\Gamma)$ gives the pdf of a charged phospholipid of certain conformation Γ

$$\rho(\Gamma) = \frac{\exp(-H_{N_P}(\Gamma))}{Q} \tag{13}$$

where $Q = \sum_\Gamma \exp(-H_{N_P}(\Gamma))$ is the partition function of the system that inaccurately expressed as a sum of the Hamiltonian of all conformations, and $-\ln Q$ is the total free energy of the system at equilibrium.

After normalization the effective Hamiltonian $H_{N_P}(\Gamma)$ expressed in units kT is given by

$$\begin{aligned}\frac{H_{N_P}(\Gamma)}{kT} &= H_P^{intra}(\Gamma)+(N-1)\int d\mathbf{r}\left[u_{int}^{H}(\Gamma,\mathbf{r})\langle c_H(\mathbf{r})\rangle+u_{int}^{T}(\Gamma,\mathbf{r})\langle c_T(\mathbf{r})\rangle\right]\\ &+\int d\mathbf{r}u_{int}^{T}(\Gamma,\mathbf{r})c_s(\mathbf{r})+\int d\mathbf{r}u_{int}^{H}(\Gamma,\mathbf{r})c_s(\mathbf{r})\\ &+N_P\int d\mathbf{r}\left[\langle c_H(\mathbf{r})\rangle\lambda_H+\langle c_T(\mathbf{r})\rangle\lambda_T\right]\frac{\varphi(\mathbf{r})}{2}\\ &-\int d\mathbf{r}\frac{\ln\phi_s(\mathbf{r})}{v_s}\left\{\langle\phi_H(\mathbf{r})\rangle+\langle\phi_T(\mathbf{r})\rangle+\phi_S(\mathbf{r})-\phi_0\right\}\end{aligned} \tag{14}$$

Eqs (9, 10, 11, 13 and 14) form a closed set of non-linear equations of the self-consistent SCMF-PBE theory. The equations are solved by replacing the integrals with the sums after the space being discretized according to the geometry of the system, and the conformation of a single molecule and the corresponding short range field potential are generated and stored before solving the system of nonlinear equations[39].

The solution of the closed set of non-linear equations of the self-consistent SCMF-PBE theory gives the profiles of the charged phospholipid membranes such as the concentration of H beads, and the probabilities of each conformation of the charged phospholipid molecules. It also gives the distribution of the solvent and mobile ions in the box.

Finally, the free energy of the system F_{sys} is related to the free energy of the simulation box minus the entropy of the solvent and mobile ions

$$F_{sys} = F - V\frac{\phi_0}{v_s}\log\left(\frac{\phi_0}{v_s}\right)+2Vc_\infty\log c_\infty \tag{15}$$

The last two terms on the right-hand side of Eq.15 can be expressed as the free energy in a reference state in which only solvent and mobile ions exist in the simulation box. Since the integral in total free energy Eq.(1) diverges for large systems,[54] considers the excess semi-grand potential with respect to reservoir by $-2Vc_\infty\log c_\infty$ which is corresponding to the third term on the right-hand side of Eq.(15).

3 Numerical Implemetation And Results Discussion

In this work we have implemented the SCMF-PBE in C++. The program consists of three modules. The first module is the sampling generator which generates the molecules conformations via Rosenbluth algorithm[55] and calculates the volumes and interactions. The second module employ Newton-Rapson method to solve the uncoupled PBE, and the solution is transferred to the third module which is based on the fixed-point iteration technique. In our program OpenMP parallelization technique is employed in solving the SCMF-PBE equations, and the program runs on 48 cores Xeon E5-2690 platform.

3.1 Modeling the Charged Phospholipid Membrane in Electrolyte Solution

Our theoretical model deliver the equilibrium properties of the system such as the volume fraction profiles of the lipids in the bilayer, the electrostatic potential and the mobile ion distribution around the charged bilayer. The equations of the previous section also allow us to calculate the free energy of the system containing a charged phospholipid bilayer in the electrolyte.

We perform the simulation of a charged phospholipid bilayer, which is convenient to study the deformation of bilayers when the interactions with nanometer-scale objects are taken into account, such as the interaction with protein domains. Furthermore, as electrostatic effects play key role in multiple interactions such as hydrophobic and hydrophilic interactions, the self-consistent SCMF-PBE theory can form the basis for another type of simulation besides Brownian dynamics (BD) and molecular dynamics (MD). Our discussion therefore focuses on the electrostatic properties of the bilayer, with consideration of the influence of the salt density on the bilayer thickness along the bilayer, and the influence of the salt concentration on the interfacial area since the free energy of a homogenous bilayer is proportional to the membrane surface area[39].

The mean-field space is divided into nested concentric circular shells of radius r and slices in cylindrical fields. We adapted the configuration model proposed by Pogodin and Baulin[39] and incorporated additional parameters listed in Tab.1; thus when the electrostatic interaction is neglected by setting $\lambda_H = 0$ and $c_\infty = 0$ we can get exact same equilibrium properties of the system such as the membrane thickness, and mean area per lipid (MAPL) that described in Ref.[39].

It is worthwhile to note that contact energies in Tab.1 are essentially treated as force fields of corresponding units, which are the most significant contributions to the system free energy.

We first consider the influence of salt concentration on the energy curves with different salt densities are presented in Fig.3. The influence of salt concentration on the stability of the phospholipid bilayer can be observed in the shift of the minimum free energy

Table 1 Molecular configuration parameters of the membrane model

Configuration Parameters	Values
Bead radius	4.05 (Å)
Interaction range	12.15 (Å)
Bond length	10.0 (Å)
T-T contact energy	-0.75 (kT)
H-S contact energy	-0.15 (kT)

per lipid of the system. The increase of c_∞ weaken the repulsion force between charged hydrophilic heads (H beads) , resulting in a decrease in interfacial area. We then considered the influence of salt concentration on the variation of volume fraction of the charged lipid. We decompose the volume fraction $\langle\phi_P\rangle$ into mean volume fraction of hydrophobic beads $\langle\phi_T\rangle$ and hydrophilic beads $\langle\phi_H\rangle$, as shown in Fig.4,in which the second row presents $\langle\phi_H\rangle$ in the solution with three different salt densities. The distance between two peak values of $\langle\phi_H\rangle$ (red zone) reflect the thickness of the bilayer, and the increase in the distance of the peaks of $\langle\phi_H\rangle$ indicates it contributes more strongly than that in $\langle\phi_T\rangle$ to the increase in the thickness of the phospholipid membrane. The repulsion strengths between the hydrophilic beads H is weakened due to the screening effect from the surrounding mobile ions which leads to the decreased MAPL. Then more charged hydrophilic beads H are packed crowded in each layer also cause the increased surface charge density, which gives rise to the increase of thickness of bilayer. Since the two layers are very close, usually less than 50 A, the increased repulsion force is non-negligible. Our elucidation of the change in lipid membrane thickness is strongly supported by experimental data in the literature[56,57], which indicate lipid bilayers monotonically swell with increasing salt concentration, due to the screening effect on the balance between the electrostatic repulsion and the van der Waals (vdW) attraction. To further confirm our results, we compared the thickness of the bilayers obtained by SCMF-PBE method and the thickness obtained from experimental data[56–58] (Tab.2). We also employed MD simulations to quantitatively analyze the relation between salt density and thickness of the lipid membrane, and detailed results are listed in Supporting Information SI-35.3.

In Tab.3 A^{a}_{SP} and A^{b}_{MD} present the comparison of MAPL of the bilayers obtained by SCMF-PBE method and Molecular Dynamics (MD) list in ascending order of corresponding salt concentration. In Tab.3 A^{c}_{DMPC} presents maximal and minimal APL values averaged over time, with standard deviations from 12 to 23Å.

Table 2 Comparison of the thickness of bilayers between results obtained from SCMF-PBE (SP) and experiments

Salt Concentration (M)			Thickness (nm)		
c^{a}_∞	c^{b}_{KCl}	c^{c}_{KBr}	d^{a}_{SP}	d^{b}_{KCl}	d^{c}_{KBr}
0.010	0.01	0.01	2.0 ±0.1	3.4 ±0.1	2.8 ±0.1
0.012	0.20	∼	2.2 ±0.1	3.5 ±0.1	∼
0.014	0.40	∼	2.8 ±0.1	3.6 ±0.1	∼
0.015	1.00	∼	3.0 ±0.1	3.5 ±0.1	∼
0.016	1.20	0.10	3.5 ±0.1	3.6 ±0.1	3.1 ±0.1

[a] $c_\infty = c_{\kappa l_B}/8\pi l_B^3$ is the bulk concentration of mobile ions in unit of M.
d_{SP} denotes the thickness of the bilayers generated by SCMF-PB method.
[b] DLPC (12-carbon-chain) bilayers in the presence of KCl at 15°C. Experimental data from[56].
[c] DDPC (10-carbon-chain) bilayers in the presence of KBr at 35°C. Experimental data from[58].

Table 3 Comparison of the MAPL (Å) of bilayers between results obtained from SCMF-PBE (SP) and MD

A^{a}_{SP}	A^{b}_{MD}	A^{c}_{DMPC}
70.0 ±0.5	51.6 ±0.5	69
64.8 ±0.5	51.9 ±0.5	∼
61.8 ±0.5	49.8 ±0.5	∼
57.8 ±0.5	49.0 ±0.5	∼
54.6 ±0.5	49.1 ±0.5	56

[a] Obtained from SCMF-PBE, with $\lambda_H = 0.015$, c_∞=0.010,0.012,0.014,0.015,0.016(M)
[b] DPPS bilayers in the presence of KCl at 50°C, Obtained from MD. The ion concentration in the box are set 0.2, 0.8,1.5,2.0,2.5 (M), details in Supporting Information
[c] Obtained from computational analysis of DMPC bilayer[59], with sodium and chloride ions to a concentration of 0.15(M).
And the standard deviations of the local APL ranges from 12 to 23 Å.

Higher concentrations of mobile ions will also lead to the decrease of electrostatic potential of the phospholipid bilayer, as indicated by the change in color of the heat map in Fig.5. From Fig.5 it can also be observed that when $c_\infty = 4.0 \times 10^{-3}$M the outline of the potential does not appear as a bilayer, due to the compressed state of the bilayer in a solution with low salt density.

However in the final plot in which $c_\infty = 1.0 \times 10^{-2}$M the outline of the bilayer is comparable with the volume fraction profile $\langle \phi_H \rangle$ at $c_\infty = 1.0 \times 10^{-2}$M plotted in Fig.4.

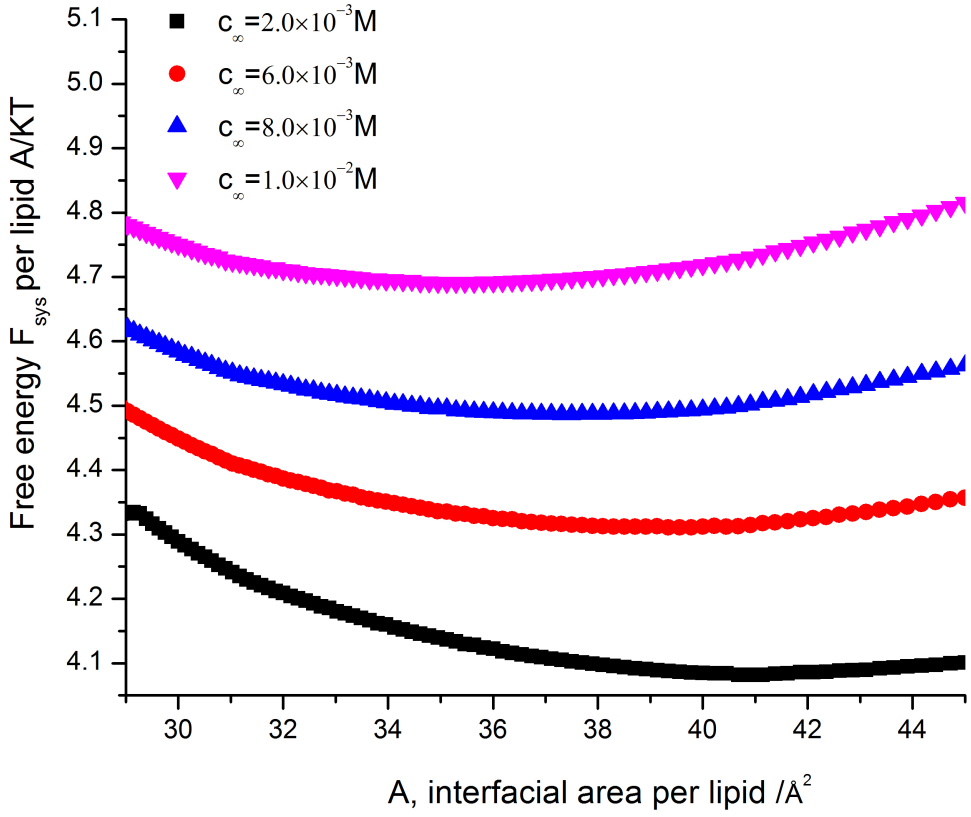

Fig. 3 Free energy F_{sys} per lipid in solution with dimensionless salt concentration (c_∞) range from 2.0×10^{-3}M to 1.0×10^{-2}M, the minimum free energy corresponding to the most probable conformations of the layer in equilibrium and the density profiles shifts to the right.

We then consider the influence of different surface charge densities on the equilibrium properties of the system. Since the charge ratio of the hydrophilic heads λ_H is an important electric property that determines the surface charge density of the lipid, different lipids can have varying quantities of charge, such as pyrophosphate lipids and phosphatidylglycerol lipids. We can create a lipid with certain surface charge density by adjusting the charge ratio of the corresponding hydrophilic heads. The energy curves with different charge ratio of H beads are presented in Fig.6, and the values of MAPL corresponding to the minimum free energy indicate lipids with higher charge density occupy more space on the surface of membrane. The dimensionless salt density is set $c_\infty = 1.9 \times 10^{-4}$M, and the results obtained from the sampling of 1 million conformations. From Fig.7, we observed the thickness decreased when $\lambda_H = 0.003$, and this is due to fewer lipids assemble into membranes. Although each lipid carry more charge with higher λ_H, the charge density in two layers still decreases that results in the repulsion force decrease even more, therefore the thickness of lipid bilayer decreases.

3.2 Interactions between Nanospheres on Charged Phospholipid Membrane

We consider interactions of two charged spherical inclusions in or stick to the charged membrane surrounded by mobile ions and charged lipid molecules. Sabyasachi[60] calculated deformation and adhesion energies as a function of membrane elastic parameters and adhesion strength, and John Lekner[61] proved that two charged conducting spheres will almost always attract each other at close approach, even when they have like charges. Here we investigate the attraction-repulsion property of two charged nanoparticles which are stuck on the charged lipid molecules surrounded with mobile ions. For conveniently we consider 3D SCMF-PBE, in our 3D physical model two charged spheres with a variety of distance on x axis are placed near the surface of the membrane, and we observe the

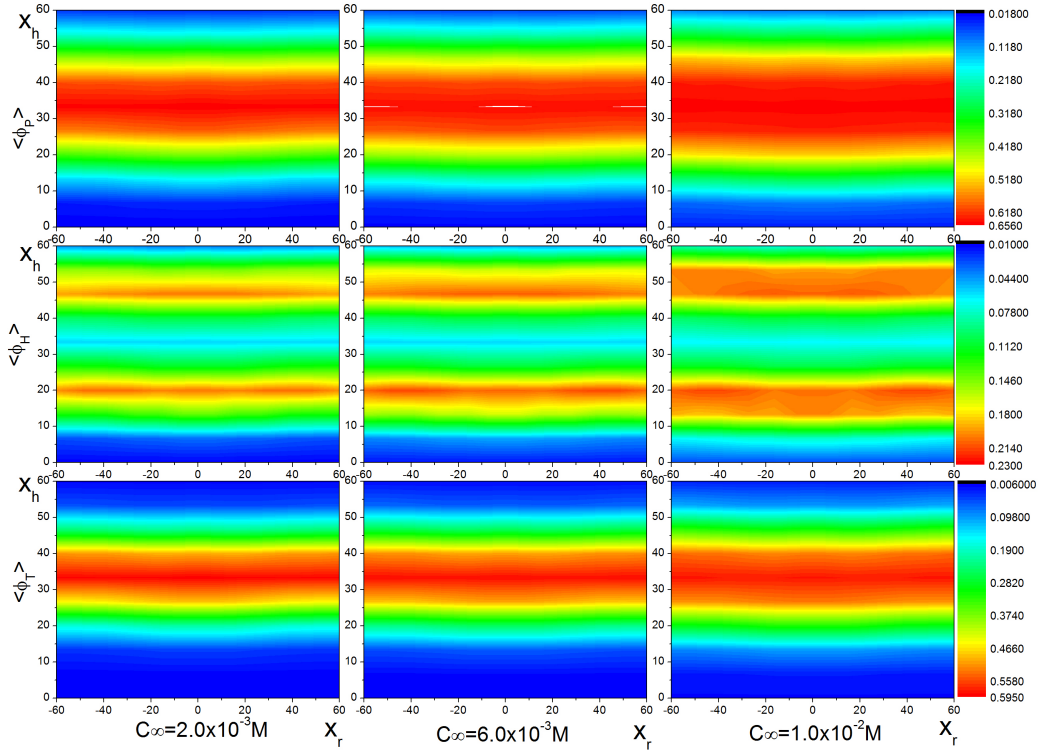

Fig. 4 Mean volume fraction profiles of $\langle\phi_P\rangle$, $\langle\phi_T\rangle$ and $\langle\phi_H\rangle$ in solution with increasing salt density from $c_\infty = 2.0\times10^{-3}M$ to $1.0\times10^{-2}M$. The mean volume fractions $\langle\phi_P\rangle$, $\langle\phi_H\rangle$ and $\langle\phi_T\rangle$ are list from the first to the third row respectively. The first row illustrates the thickness of the lipid bilayer (red part) increases with salt density increasing.

variation of the system energy and profiles of the two spheres. The 3D SCMF-PBE equations and corresponding boundary conditions are list in SI-2 5.2.

Fig.8 shows the energies as a function of the distance D between two identical charged spheres, and it shows that two charged spheres attract each other at close approach. We observe the energy increases again with distance D continues increasing because of periodic boundary condition in which two spheres approach the boundary of the simulation box respectively. One similar unusual phenomenon of attraction between conducting spheres carrying like charges is proved theoretically[61]. Another similar phenomenon of attraction between two charged cylinders is discussed numerically, although different amount of charge carried by two charged cylinders[53]. And the figures of the electrostatic potential of the system with two charged sphere at 4 distances are shown in Fig.9, and it is noted these figures are taken at the membrane surface $z = 27$ Å.

3.3 Interaction of Nanoparticles and Proteins with Charged Phospholipid Membrane

In our study we simulate the interaction between the Akt PH domain and the cytoplasmic membrane as an application. Akt is a crucial oncogene that has been implicated in a variety of cancer and it is involved in the tumorigenesis and metastasis. PH domains is a protein domain (part of protein) of approximately 120 amino acids which are found for translocation and activation around the cell membrane. For this function, the PH domain needs to bind phosphatidylinositol lipids (e.g. PIP3) to form a complex, in which phosphatidylinositol lipids are negatively charged compounds in a cylindrical shape. For simplicity and clarity, a coarse-grained model is employed in which the PH domain protein is represented by a charged sphere with radius 8Å, and PIP3 is represented by a short cylinder with length 10(Å) and attached to the charged sphere; the interaction between the lipids is also taken into consideration. From experiment we know that some complex that composed by PIP3 or PIP2 and some PH Domain protein may bind to membrane eventually by inserting the PIP3 or PIP2 into the membrane[62], while some are not. The quantitative comparison of the electrostatic free energy of interaction of the system composed by PLC(a PH domain protein) and PIP2 and the system composed by PLC and PIP3 with the distance between the van der Waals surfaces of the PLC and membrane exhibits the attraction-repulsion respectively[63], and it has been proved by[64]. We are interested

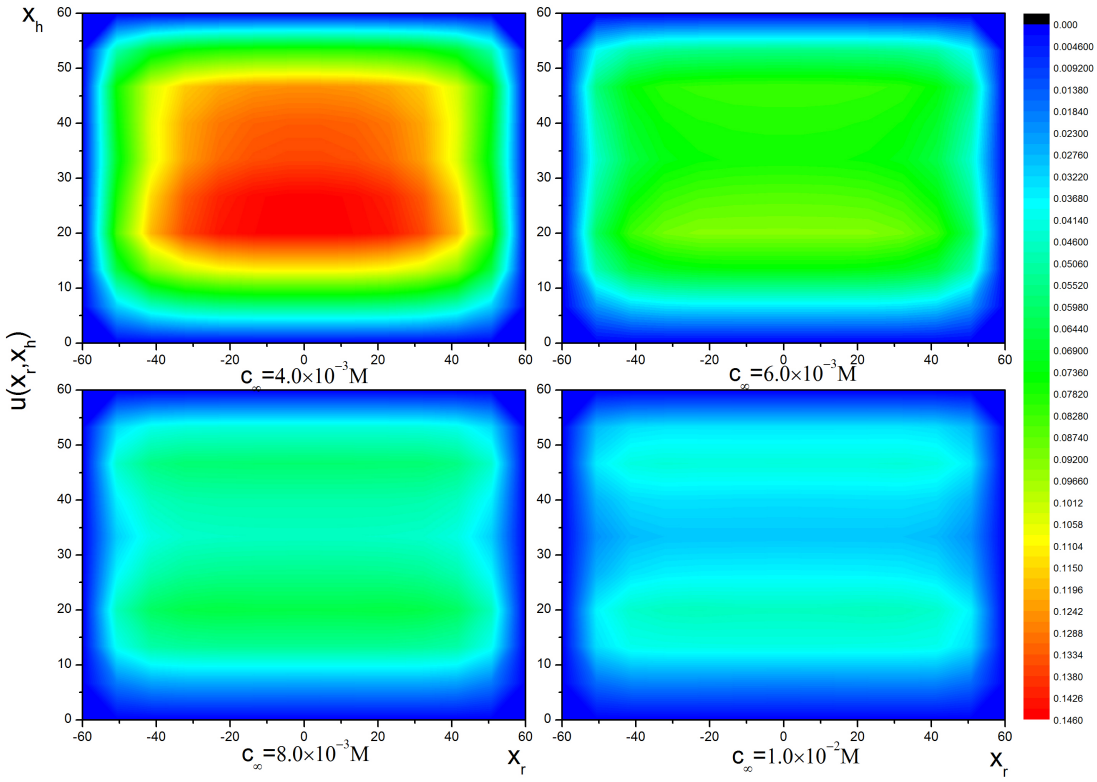

Fig. 5 The variation of the electrostatic potential in solution with increasing salt density.

in the procedure of the Akt PH domain with PIP3 binding to the membrane, and the binding affinity of the complex to the membrane will affect our choice of certain phosphatidylinositol lipids (PIP2 or PIP3) in future application. As shown in Fig.10, the model simulates the whole process of the PH-domain protein's approaching the membrane and PIP3's insertion into the membrane to reach equilibrium. The images in the first row of Fig.10 present the mean volume fraction of the coarse-grained phosphatidylinositol lipids, and the bottom of corresponding snapshots are viewed form overall perspective. This figure exhibits the process of the PH-domain protein (green ball) approaching the membrane and the insertion of PIP3 (pink cylinder) into the membrane.

As shown in the second row of Fig.10, the variation of the free energy of the system F_{sys} in the simulation of the interaction indicates PIP3 inserting the membrane and the PH-domain protein stick to the interface of the membrane in equilibrium. Although quantitative evidence for PH-domain protein is scarce, a lot qualitative analysis demonstrate the effectiveness of our model. For example, our results are supported by the in vitro experiments performed by Seo[30] et al, who showed that charge-shielding by free cations modulated the binding of phospholipase C (PLC) to the membrane phospholipid PIP2. PLC interacts with PIP2 via the enzyme's PH domain; this interaction is analogous to the interaction of a generic charged lipid (pink cylinder in Fig.10) with a generic charged protein (green sphere in Fig.10) in our simulations.

Furthermore, our simulations indicated that the lowest-energy state for a charged protein would be close to the membrane, a result that is supported by cellular studies examining the translocation of PLC from the cytosol to the plasma membrane. Wang[65] showed in a mammalian cell system that the PH domain stabilizes the interaction of PLC with the plasma membrane, indicating that the lowest-energy state would place the PH domain and the membrane lipids close together. All this demonstrates a potential application in membrane protein modeling and design.

Another interesting phenomenon we observed in our simulation is that the pore formed by the PH domain disappears gradually as the salt density increases. As shown in Fig.11, we observed that the increasing concentration of mobile ions weaken the steric repulsion force between the lipids and allow more lipids per unit volume to assemble. Analogously, the left column of Fig.11 lists the mean volume fraction of the coarse-grained phosphatidylinositol lipids, and the right column lists the corresponding snapshots viewed form top-down perspective, which demonstrates the pore disappearing as the salt density increases. Our results also predict that as the concentration of salt is increased, the repulsion between individual lipids of the membrane would be weakened due to the screening

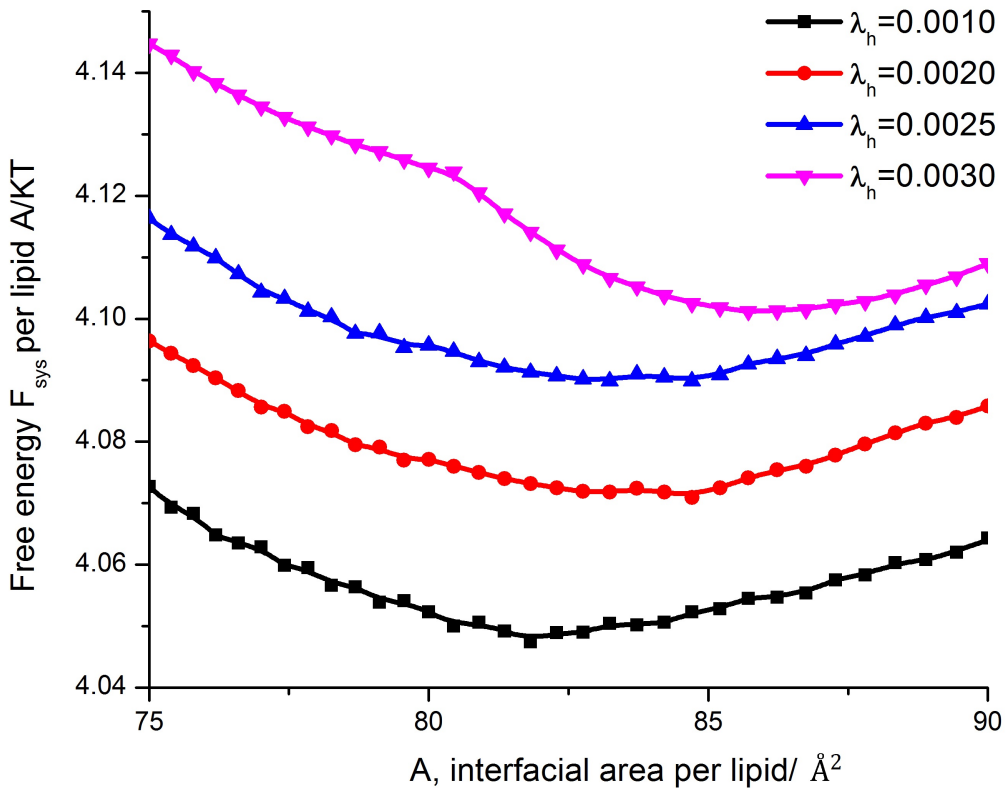

Fig. 6 Free energy of the system per lipid area A, the phospholipid molecules H_1T_2 are with different charge ratio λ_H, and the dimensionless salt density is fixed $c_\infty = 2.0\times10^{-4}$M

effect. This prediction has been confirmed in wet-laboratory experiments by Carmona-Ribeiro[66].

4 Conclusions

The present approach incorporated the Single Chain Mean Field theory with Poisson Boltzmann theory to explore the equilibrium properties of charged phospholipid membranes. In addition we considered the influence of mobile ions on the membrane thickness, the APL and the corresponding electrostatic potential. We simulated the interaction between Pleckstrin homology domain of Akt and cytoplasmic membrane with coarse grained model. The study of pore formation by the charged proteins is a promising research field in which the reasons for the activation of oncogenic proteins would be possible.

5 Appendix

5.1 SI-1

In our model the space of the simulation box is discretized into concentric circular shells of radius r and layers or slices along z axis in a 2D cylindrical fields. In this 2D $r-z$ coordinates, $\varphi(r,z)$ represents the electrostatic potential at cell (r,z), and the differential Poisson-Boltzmann equation is written

$$\frac{\partial\varphi(r,z)}{r\partial r}+\frac{\partial^2\varphi(r,z)}{\partial r^2}+\frac{\partial^2\varphi(r,z)}{\partial z^2} = -\frac{4\pi q}{\varepsilon}\langle\rho_{total}(r,z)\rangle \tag{16}$$

where q denotes the elementary charge and ε is the solvent dielectric constant, and $\langle\rho_{total}(r,z)\rangle$ is the mean total charge density described in Eq.8. In our 2D model, the space of the box is divided into concentric circular shells of thickness δ_h and layers of slices with thickness δ_r , then $x_h=\frac{z}{\delta_h}$, $x_r=\frac{r}{\delta_r}$. For brevity in computation we set dimensionless electrostatic potential $u(x_r,x_h)=\beta q\varphi(x_r,x_h)$, and

$$\langle\rho_{total}(x_r,x_h)\rangle=\langle c_H(x_r,x_h)\rangle\lambda_H+\langle c_T(x_r,x_h)\rangle\lambda_T \tag{17}$$

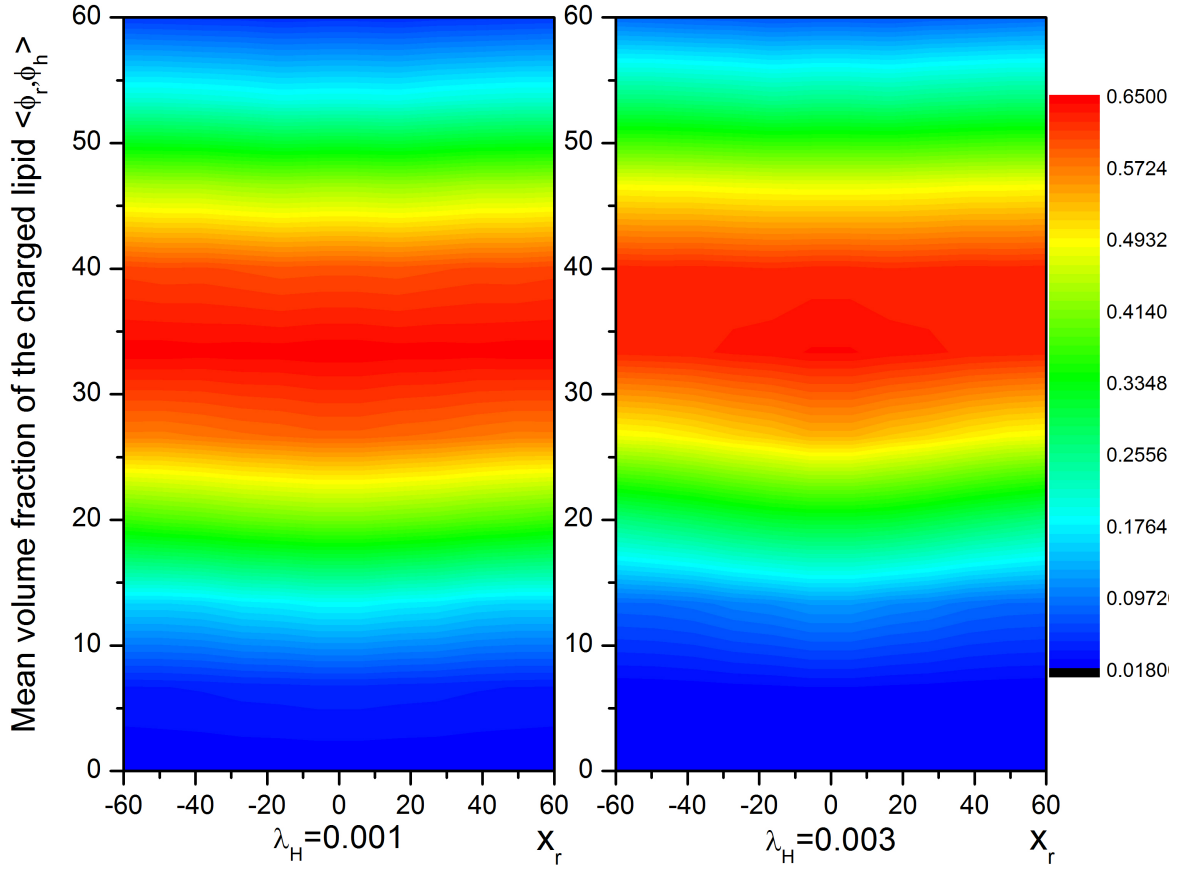

Fig. 7 The volume fraction of phospholipid membrane in the simulation box. The membranes are assembled by the phospholipids with different charge ratios $\lambda_H = 0.002$ and $\lambda_H = 0.003$.

then the 2D differential Poisson-Boltzmann equation

$$\frac{\partial u(x_r,x_h)}{x_r \partial x_r} + \frac{\partial^2 u(x_r,x_h)}{\partial x_r^2} + \frac{\partial^2 u(x_r,x_h)}{\partial x_h^2}\left(\frac{\delta_r}{\delta_h}\right)^2 = -4\pi\delta_r^3 N_P\left[\langle c_H(x_r,x_h)\rangle\lambda_H + \langle c_T(x_r,x_h)\rangle\lambda_T\right]/\left(\frac{\delta_r}{l_B}\right) + \frac{c_{\kappa l_B}}{2}\left(\frac{\delta_r}{l_B}\right)^2\left[e^{u(x_r,x_h)} - e^{-u(x_r,x_h)}\right]$$

where $\left(\frac{\delta_r}{\delta_h}\right)$ and $\left(\frac{\delta_r}{l_B}\right)$ are two ratios determined by the input parameters. N_P is the number of phospholipid molecules, and $c_{\kappa l_B} = (\kappa l_B)^2$ is proportion to the salt density which can be used for tuning the salt density in the solution. Inverse Debye length $\frac{1}{\kappa}$ is defined by $l_B c_\infty = \frac{\kappa^2}{8\pi}$, and $l_B = \frac{\beta q^2}{\varepsilon}$ is the Bjerrum length and ε is the solvent dielectric constant. where $(\kappa l_B)^2$ is a parameter which is proportional to the salt density, and $\frac{\delta_r}{l_B}$ is the ratio of the thickness to the Bjerrum length, which is a constant in the numerical test we set it 2.0. Finally, discretization of the boundary Γ with the Dirichlet boundary condition are

$$u(x_r, x_{h=0}) = 0, u(x_r, x_{h=max}) = 0 \tag{18}$$

and

$$u(x_{r=max}, x_h) = 0, u'(0, x_h) = 0 \tag{19}$$

where $x_{h=max}$ and $x_{h=0}$ corresponds to the heights of the top layer and bottom layer, and $x_{r=max}$ is the radius of the outermost layer of the nested cylinder.

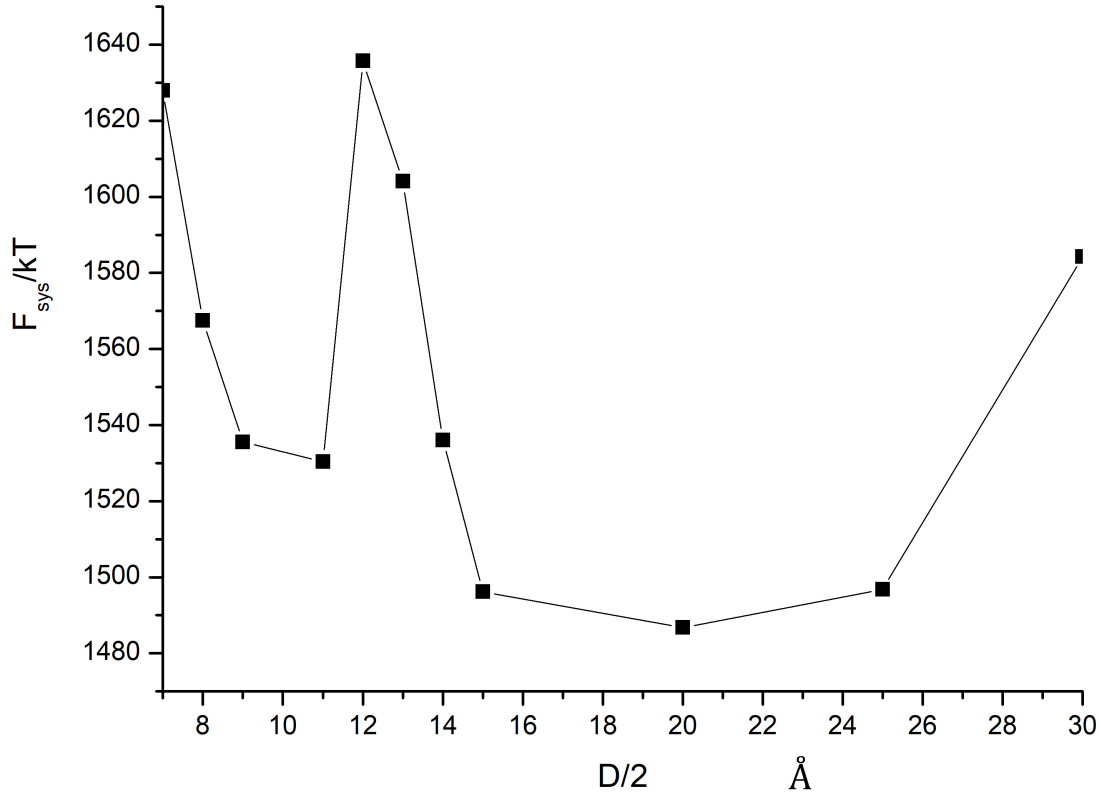

Fig. 8 The variation of the energy of the system F_{sys} as a function of the distance D Å between two charged spheres. The rise of system energy F_{sys} at close approach of these two charged spheres indicates the interaction transition from attraction to repulsion during the departure of them. Due to periodic boundary condition, the energy increases again when the spheres apart far away from each other and approach the boundaries of the box respectively.

5.2 SI-2

In our 3D model the space of the simulation box is discretized into cube fields, and $\varphi(x,y,z)$ represents the electrostatic potential at cube (x,y,z), and the 3D differential Poisson-Boltzmann equation is written

$$\frac{\partial^2\varphi}{\partial x^2}+\frac{\partial^2\varphi}{\partial y^2}+\frac{\partial^2\varphi}{\partial z^2} \quad = \quad -\frac{4\pi}{\varepsilon}\left\langle\rho_{total}(x,y,z)\right\rangle \tag{20}$$

where

$$\left\langle\rho_{total}(x,y,z)\right\rangle \quad = \quad \left\langle c_H(x,y,z)\right\rangle\lambda_H+\left\langle c_T(x,y,z)\right\rangle\lambda_T+c_\infty\left\{e^{-\beta q\varphi(x,y,z)}-e^{\beta q\varphi(x,y,z)}\right\}$$

where q denotes the elementary charge and ε is the solvent dielectric constant, and $\left\langle\rho_{total}(x,y,z)\right\rangle$ is the mean total charge density described in Eq.8 still. For brevity in computation we set dimensionless electrostatic potential $u(x,y,z)=\beta q\varphi(x,y,z)$, and we denote $\frac{x}{l_B}$ by x, denote $\frac{y}{l_B}$ by y and denote $\frac{z}{l_B}$ by z, we can obtain Eq.21.

$$\frac{\partial^2u}{\partial x^2}+\frac{\partial^2u}{\partial y^2}+\frac{\partial^2u}{\partial z^2} \quad = \quad -4\pi l_B^3N_P\left[\left\langle c_H(x,y,z)\right\rangle\lambda_H+\left\langle c_T(x,y,z)\right\rangle\lambda_T\right]+\frac{c_{\kappa l_B}}{2}\left\{e^{u(x,y,z)}-e^{-u(x,y,z)}\right\} \tag{21}$$

where N_P is the number of charged phospholipid molecules, and $l_B=\frac{\beta q^2}{\varepsilon}$ is the Bjerrum length and ε is the solvent dielectric constant. $c_{\kappa l_B}=(\kappa l_B)^2$ is proportion to the salt density that be used for tuning the salt density in the solution. Boundary Γ consists of 6 sides,

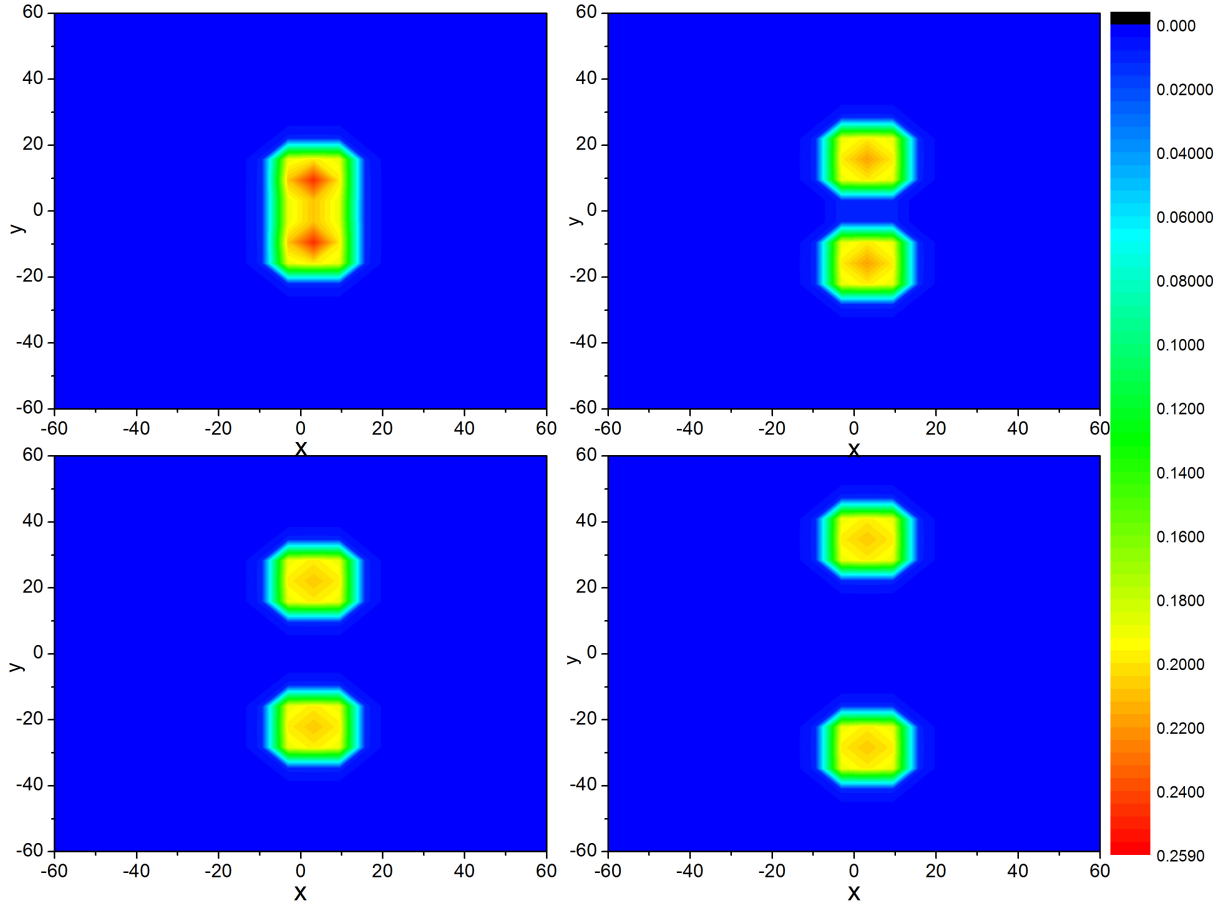

Fig. 9 The variation of the electrostatic potential of the system during the departure of two charged spheres with radius 6 Å, with between distance $D/2 = 7,13,20$ and 30 Å respectively, and at $z = 27$ Å

therefore discretization of the boundary Γ with the Dirichlet boundary condition are

$$u(x = \pm x_{max}, y, z) = 0, u(x, y = \pm y_{max}, z) = 0, u(x, y, z = \pm z_{max}) = 0 \tag{22}$$

where x_{max}, y_{max} and z_{max} are the cutoff lengths on axis x,y and z respectively.

5.3 SI-3

The Molecular dynamics (MD) simulations are executed by Gromacs (version 5.1.4), and the structure of the charged membrane built by the lipid DPPS via tool The Membrane Builder[67–69]. The simulation used forcefield charmm36 for lipids, and TIP3P water model. The simulation temperature was maintained 323.15 K. The simulation pressure (compressibility) was maintained at 1 bar. Periodic boundary condition (PBC) were employed, and the particle mesh Ewald (PME) was used for electrostatic interactions with coulomb range 1.2 nm. The simulation time step was set to 2 fs with the SHAKE algorithm to constrain the covalent bonds involving hydrogen atoms via LINCS algorithm.

The obtained data are analyzed by tool GridMAT-MD, which is designed to analyze thickness and area per lipid headgroup (APL) in simulations of lipid bilayers[70]. Fig.12 illustrate the thickness of the charged membrane assembled by lipid DPPS. The simulation executed in a rectangular box with size 100×100, and the salt density in solution vary from 0.2 to 2.5

Conflicts of interest

There are no conflicts to declare.

Acknowledgements

The authors are grateful to Prof. Vladimir Baulin, Prof. Benzhuo Lu and Mr. Lon Wolf Fong. SZ and BH are partially supported by Cancer Prevention and Research Institute of Texas (CPRIT) grants DP150086 and RP170333, National Science Foundation (NSF) grant

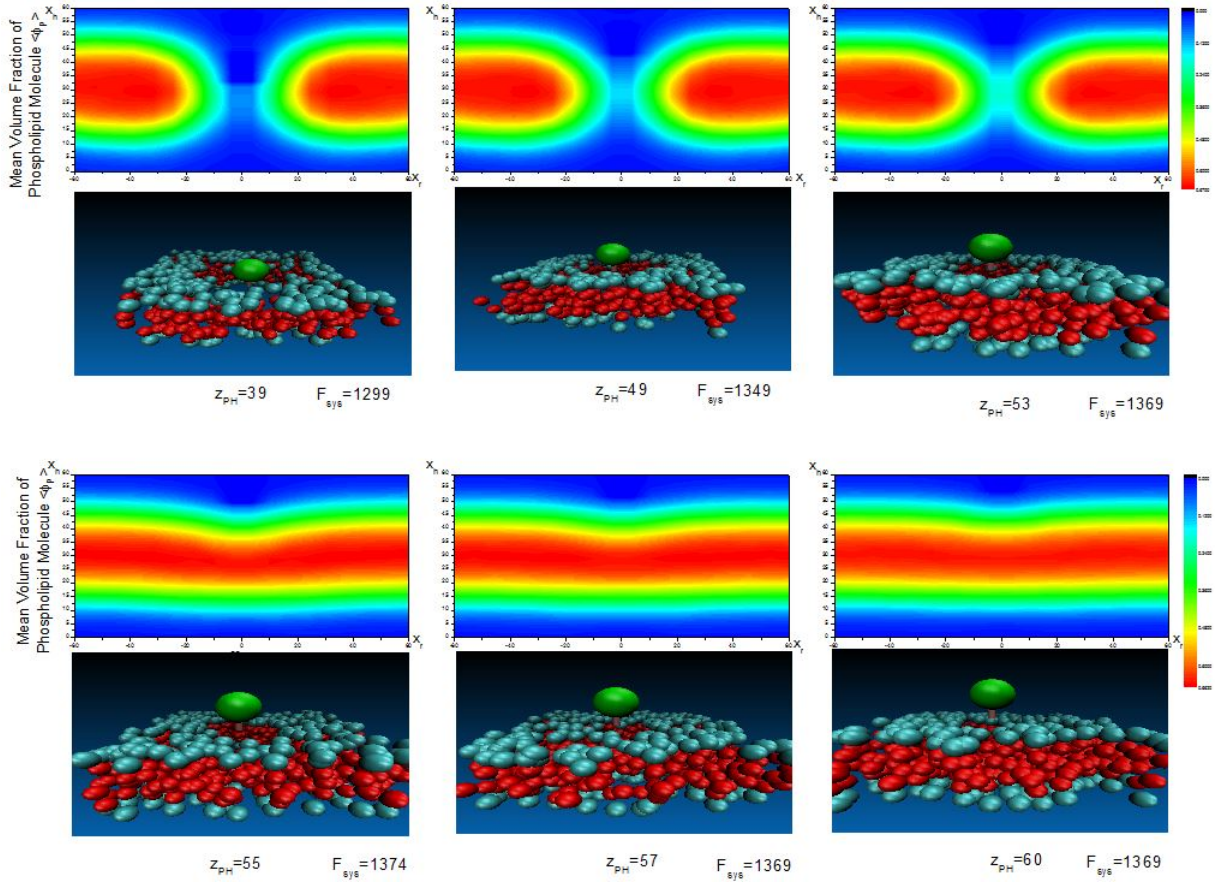

Fig. 10 The variation of the mean volume fraction profiles of lipid $\langle\phi_P\rangle$, and corresponding snapshot are list below. The green sphere represents Domain Protein with dimensionless surface charge density 1.0×10^{-5}, and the attached pink cylinder represents the pip3 with dimensionless surface charge density 1.0×10^{-6}. z_{PH} denotes the center of the pip3 in coordinate Z, and the free energy of the system F_{sys} gradually increases during the PH Domain Protein rising up.

CHE-1411859, and the Institutional Research Grant (IRG) Program at The University of Texas MD Anderson Cancer Center. Special thanks to the Texas Advanced Computing Center (TACC) at The University of Texas at Austin for providing high-performance computing resources for this study.

Notes and references

1 T. E. Andreoli, J. F. Hoffman, D. D. Fanestil and S. G. Schultz, *Membrane Physiology*, Springer US, Boston, MA, 1987.
2 L. S. Van Winkle, Z. A. Johnson, S. J. Nishio, C. D. Brown and C. G. Plopper, *American Journal of Respiratory Cell and Molecular Biology*, 1999, **21**, 44–53.
3 S. S. Panda, P. Mohapatra and R. Mohanty, *Microbiological Research*, 1999, **153**, 363–368.
4 J. Mathieu-Denoncourt, S. J. Wallace, S. R. de Solla and V. S. Langlois, *Bulletin of Environmental Contamination and Toxicology*, 2016, **97**, 4–10.
5 L. Q. Shen, J. Nan and B. Lu, *Sustainable Chemistry & Engineering*, **6**, 2055–2061.
6 W. Zhao, S. Prijic, B. C. Urban, M. J. Tisza, Y. Zuo, L. Li, Z. Tan, X. Chen, S. A. Mani and J. T. Chang, *Cancer Research*, 2016, **76**, 2037–2049.
7 B. Hu, Q. Wang, Y. A. Wang, S. Hua, C.-E. G. Sauvĺe, D. Ong, Z. D. Lan, Q. Chang, Y. W. Ho, M. M. Monasterio, X. Lu, Y. Zhong, J. Zhang, P. Deng, Z. Tan, G. Wang, W.-T. Liao, L. J. Corley, H. Yan, J. Zhang, Y. You, N. Liu, L. Cai, G. Finocchiaro, J. J. Phillips, M. S. Berger, D. J. Spring, J. Hu, E. P. Sulman, G. N. Fuller, L. Chin, R. G. Verhaak and R. A. DePinho, *Cell*, 2016, **167**, 1281–1295.e18.
8 T. Zhi, L. Yanhong, L. Rui, S. Jian, L. Jinping and W. Junzhu, *European Journal of Lipid Science and Technology*, 2012, **114**, 880–888.
9 C.-F. Su, H. Merlitz, H. Rabbel and J.-U. Sommer, *The Journal of Physical Chemistry Letters*, 2017, **8**, 4069–4076.
10 V. Garcia-Lopez, F. Chen, L. G. Nilewski, G. Duret, A. Aliyan, A. B. Kolomeisky, J. T. Robinson, G. Wang, R. Pal and J. M. Tour, *Nature*, 2017, **548**, 567–572.
11 Z. Tan, L. Chen and S. Zhang, *Scientific Reports*, 2016, **6**, 33534.

12 Z. Tan, R. Chaudhai and S. Zhang, *ChemMedChem*, 2016, **11**, 1211–1218.
13 A. S. Reddy, Z. Tan and S. Zhang, *Journal of Chemical Information and Modeling*, 2014, **54**, 2536–2543.
14 R. Chaudhari, Z. Tan, B. Huang and S. Zhang, *Expert Opinion on Drug Discovery*, 2017, **12**, 279–291.
15 J. N. Israelachvili, *Intermolecular and surface forces*, Academic Press, Burlington, MA, 3rd edn, 2011.
16 R. A. Rozendal, T. H. J. A. Sleutels, H. V. M. Hamelers and C. J. N. Buisman, *Water Sci. Technol.*, 2008, **57**, 1757–1762.
17 C. R. Dias and M. N. de Pinho, *Journal of Molecular Liquids*, 1999, **80**, 117–132.
18 E. Gongadze, K. Bohinc, U. van Rienen, V. Kralj-Iglic and A. Iglic, *Advances in Planar Lipid Bilayers and Liposomes*, Elsevier, 2010, vol. 11, pp. 101–126.
19 S. Perutkova, M. Frank, K. Bohinc, G. Bobojevic, J. Zelko, B. Rozman, V. Kralj-Iglic and A. Iglic, *The Journal of Membrane Biology*, 2010, **236**, 43–53.
20 K. Bohinc, J. J. Giner-Casares and S. May, *J. Phys. Chem. B*, 2014, **118**, 7568–7576.
21 K. Bohinc, G. V. Bossa and S. May, *Advances in Colloid and Interface Science*, 2017, **249**, 220–233.
22 S. McLaughlin, *Annu. Rev. Biophys. Biophys. Chem.*, 1989, **18**, 113–136.
23 *Structure and dynamics of membranes*, ed. R. Lipowsky and E. Sackmann, Elsevier Science, Amsterdam; New York, 1995.
24 Y. Levin, *Rep. Prog. Phys.*, 2002, **65**, 1577.
25 M. Muller, K. Katsov and M. Schick, *Physics Reports*, 2006, **434**, 113–176.
26 M. Venturoli, M. Maddalenasperotto, M. Kranenburg and B. Smit, *Physics Reports*, 2006, **437**, 1–54.
27 K. Bohinc, V. Kralj-Iglic and S. May, *JOURNAL OF CHEMICAL PHYSICS*, 2003, **119**, 7435–7444.
28 A. G. Cherstvy and E. P. Petrov, *Phys. Chem. Chem. Phys.*, **16**, 2020–2037.
29 S. K. Ghosh, A. G. Cherstvy, E. P. Petrov and R. Metzler, *Soft Matter*, **12**, 7908–7919.
30 J. B. Seo, S.-R. Jung, W. Huang, Q. Zhang and D.-S. Koh, *PLOS ONE*, 2015, **10**, e0144432.
31 Y. Ma, Y. Yamamoto, P. R. Nicovich, J. Goyette, J. Rossy, J. J. Gooding and K. Gaus, *Nature Biotechnology*, 2017, **35**, 363–370.
32 R. Goetz and R. Lipowsky, *The Journal of Chemical Physics*, 1998, **108**, 7397.
33 R. Goetz, G. Gompper and R. Lipowsky, *Physical Review Letters*, 1999, **82**, 221–224.
34 J. C. Shelley, M. Y. Shelley, R. C. Reeder, S. Bandyopadhyay, P. B. Moore and M. L. Klein, *The Journal of Physical Chemistry B*, 2001, **105**, 9785–9792.
35 J. C. Shelley, M. Y. Shelley, R. C. Reeder, S. Bandyopadhyay and M. L. Klein, *The Journal of Physical Chemistry B*, 2001, **105**, 4464–4470.
36 M. Muller, K. Katsov and M. Schick, *Journal of Polymer Science Part B: Polymer Physics*, 2003, **41**, 1441–1450.
37 I. R. Cooke, K. Kremer and M. Deserno, *Physical Review E*, 2005, **72**, year.
38 S. J. Marrink and D. P. Tieleman, *Chemical Society Reviews*, 2013, **42**, 6801.
39 S. Pogodin and V. A. Baulin, *Soft Matter*, 2010, **6**, 2216.
40 I. Szleifer, A. Ben-Shaul and W. M. Gelbart, *The Journal of Chemical Physics*, 1985, **83**, 3612.
41 I. Szleifer, *The Journal of Chemical Physics*, 1986, **85**, 5345.
42 A. Ben-Shaul, I. Szleifer and W. M. Gelbart, *The Journal of Chemical Physics*, 1985, **83**, 3597.
43 T. Tanaka, *Phys. Rev. E*, 1998, **58**, 2302–2310.
44 H. Huang and T. Toyoizumi, *Phys. Rev. E*, 2015, **91**, 050101.
45 A. Gezae Daful, V. A. Baulin, J. Bonet Avalos and A. D. Mackie, *The Journal of Physical Chemistry B*, 2011, **115**, 3434–3443.
46 S. Poyry and I. Vattulainen, *Biochimica et Biophysica Acta (BBA) - Biomembranes*, 2016, **1858**, 2322–2333.
47 A. D. Mackie, A. Z. Panagiotopoulos and I. Szleifer, *Langmuir*, 1997, **13**, 5022–5031.
48 Z. A. Al-Anber, J. Bonet Avalos and A. D. Mackie, *The Journal of Chemical Physics*, 2005, **122**, 104910.
49 D. Andelman, *Handbook of Biological Physics*, North-Holland, 1995, vol. 1, pp. 603–642.
50 J.-L. Barrat and F. Joanny, *Advances in Chemical Physics*, John Wiley & Sons, Inc., Hoboken, NJ, USA, 1996, vol. 94, pp. 1–66.
51 C. Fleck, R. R. Netz and H. H. von Grunberg, *Biophysical Journal*, 2002, **82**, 76–92.
52 N. Laanait, *Ion correlations at electrified soft matter interfaces*, Springer, Cham, 2013.
53 B. Huang, S. Maset and K. Bohinc, *The Journal of Physical Chemistry B*, 2017, **121**, 9013–9023.
54 V. A. Baulin and E. Trizac, *Soft Matter*, 2012, **8**, 6755–6766.
55 M. N. Rosenbluth and A. W. Rosenbluth, *The Journal of Chemical Physics*, 1955, **23**, 356–359.
56 H. I. Petrache, T. Zemb, L. Belloni and V. A. Parsegian, *Proceedings of the National Academy of Sciences*, 2006, **103**, 7982–7987.
57 A. I. I. Tyler, H. M. G. Barriga, E. S. Parsons, N. L. C. McCarthy, O. Ces, R. V. Law, J. M. Seddon and N. J. Brooks, *Soft Matter*, 2015, **11**, 3279–3286.
58 H. I. Petrache, S. Tristram-Nagle, D. Harries, N. Kucerka, J. F. Nagle and V. A. Parsegian, *Journal of Lipid Research*, 2006, **47**,

302–309.
59 V. Gapsys, B. L. de Groot and R. Briones, *Journal of Computer-Aided Molecular Design*, 2013, **27**, 845–858.
60 S. Dasgupta, T. Auth and G. Gompper, *Soft Matter*, **9**, 5473–5482.
61 J. Lekner, *Proceedings of the Royal Society A: Mathematical, Physical and Engineering Sciences*, **468**, 2829–2848.
62 E. Yamamoto, A. Kalli, K. Yasuoka and M. Sansom, *Structure*, 2016, **24**, 1421–1431.
63 S. M. Singh and D. Murray, *Protein Science*, 2003, **12**, 1934–1953.
64 K. E. Landgraf, C. Pilling and J. J. Falke, *Biochemistry*, 2008, **47**, 12260–12269.
65 Y. Wang and Z. Wang, *Traffic*, **4**, 618–630.
66 A. M. Carmona-Ribeiro and H. Chaimovich, *Biophys. J.*, **50**, 621–628.
67 S. Jo, T. Kim and W. Im, *PLoS ONE*, 2007, **2**, e880.
68 S. Jo, T. Kim, V. G. Iyer and W. Im, *Journal of Computational Chemistry*, 2008, **29**, 1859–1865.
69 E. L. Wu, X. Cheng, S. Jo, H. Rui, K. C. Song, E. M. Davila-Contreras, Y. Qi, J. Lee, V. Monje-Galvan, R. M. Venable, J. B. Klauda and W. Im, *Journal of Computational Chemistry*, 2014, **35**, 1997–2004.
70 W. J. Allen, J. A. Lemkul and D. R. Bevan, *Journal of Computational Chemistry*, 2009, **30**, 1952–1958.

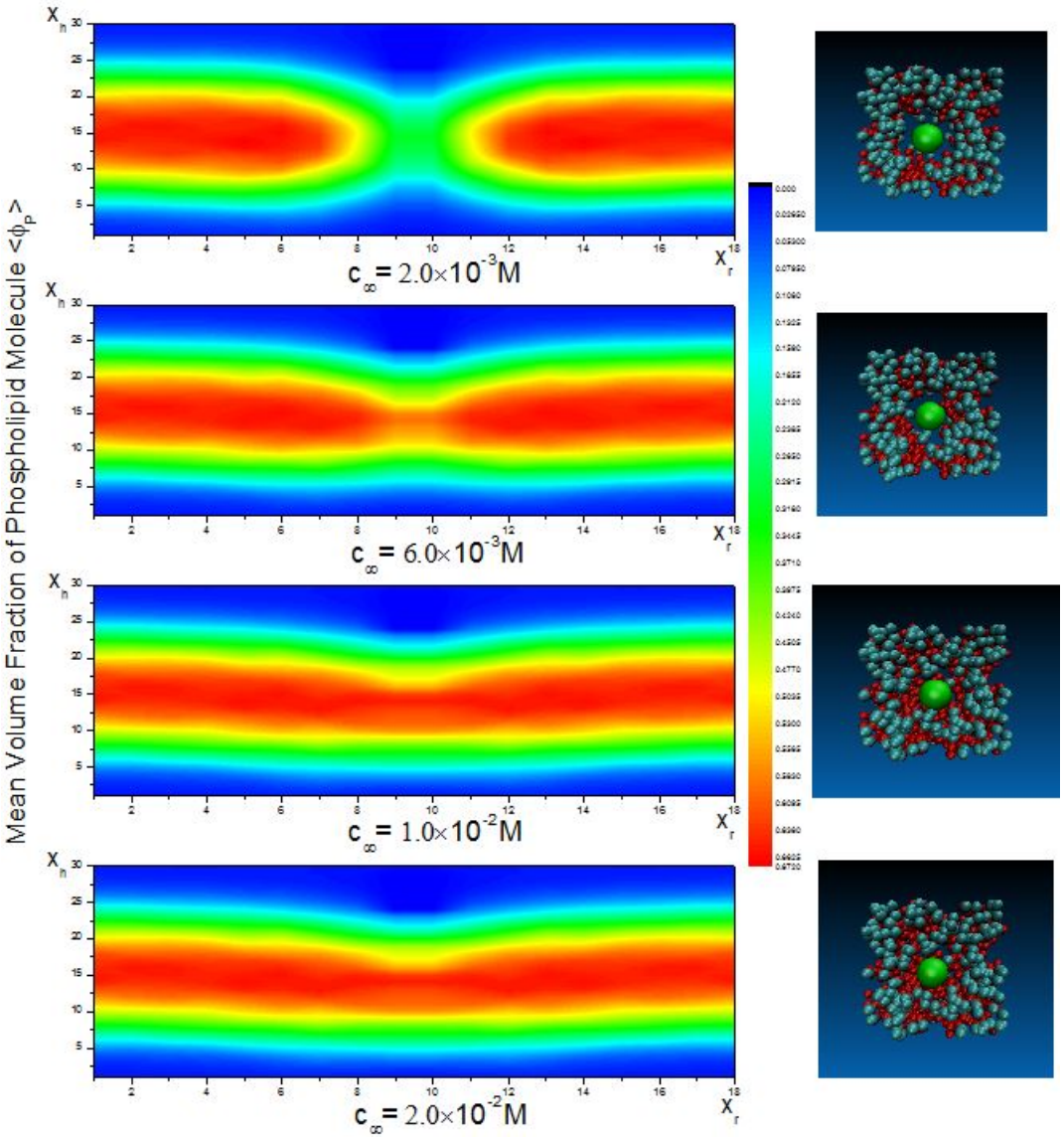

Fig. 11 The variation of the mean volume fraction profiles of lipid $\langle \phi_P \rangle$, and on the right list the corresponding snapshot in top-down perspective. The green sphere represents Domain Protein with dimensionless surface charge density 3.0×10^{-4}, and the attached pink cylinder represents the pip3 with dimensionless surface charge density 1.0×10^{-4}. The center of the pip3 is fixed at $z_{PH} = 39$. The pore of the membrane is opened up by the charged protein inserted, and with the dimensionless salt density c_∞ increases from 2×10^{-3}M to 2×10^{-2}M, and the pore disappear gradually.

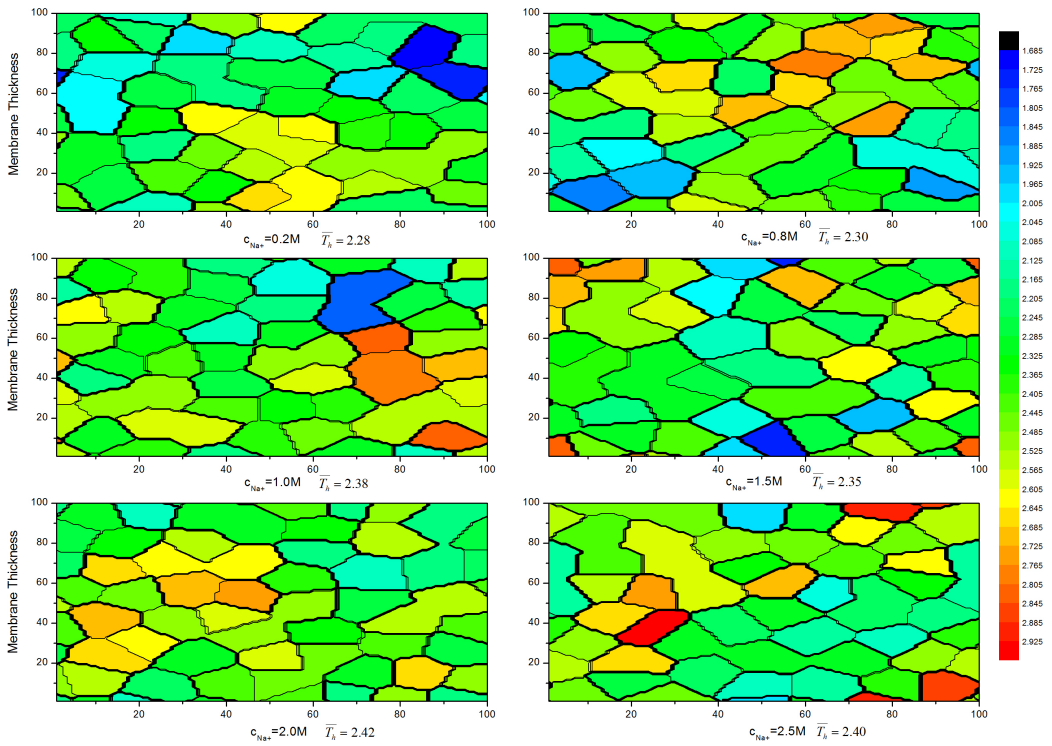

Fig. 12 Variation of the thickness of the charged membrane. T_h denote the average thickness of the membrane in the solution with corresponding salt density.